buildings

Article

Horizontal Deformation Monitoring of Concrete Pile with FRP-Packaged Distributed Optical-Fibre Sensors

Yongsheng Tang [1,*], Mengfei Cao [1], Bo Li [2], Xuhui Chen [1] and Zhenyu Wang [1]

1 College of Civil and Transportation Engineering, Hohai University, Nanjing 210098, China
2 China Design Group Corporation Limited, Nanjing 210014, China
* Correspondence: ystang_civil@hhu.edu.cn

Abstract: Horizontal deformation is a key parameter in the structural assessment of concrete piles, especially in landslide cases. However, the existing deformation-monitoring methods cannot satisfy the demands of long-term monitoring. Therefore, a new method based on distributed optical-fibre sensing technology is proposed for the long-term monitoring of the horizontal deformation of concrete piles. First, a distributed long-gauge optical-fibre sensor is embedded into a fibre-reinforced polymer (FRP) for the excellent distributed strain measurement of the concrete piles in damage cases, such as concrete cracking and reinforcement yielding. Second, based on the typical Winkler beam model, a calculation theory can be constructed for the horizontal deformation of the concrete piles with the input of the strain measurement. Lastly, the proposed method is verified via finite element simulation and static experiments in a laboratory, and the results show good accuracy. Before the case of reinforcement yielding, the largest measurement error of deformation is about 1 mm. It can be up to several millimetres after reinforcement yielding due to the large gap between the calculation model and the actual structure, while the relative measurement error is only about 10%. Due to the distributed strain measurement, the inside horizontal deformation distribution of the concrete piles can be monitored online with the proposed method to implement a detailed assessment of the pile health. Additionally, considering the excellent long-term performance of FRPs and optical-fibre sensors, the proposed method can be applied for the long-term deformation monitoring of concrete piles.

Keywords: concrete pile; horizontal deformation monitoring; FRP-packaged distributed optical-fibre sensor; distributed strain measurement; landslide

Citation: Tang, Y.; Cao, M.; Li, B.; Chen, X.; Wang, Z. Horizontal Deformation Monitoring of Concrete Pile with FRP-Packaged Distributed Optical-Fibre Sensors. *Buildings* **2023**, *13*, 2454. https://doi.org/10.3390/buildings13102454

Academic Editor: Bo-Tao Huang

Received: 29 August 2023
Revised: 21 September 2023
Accepted: 25 September 2023
Published: 27 September 2023

1. Introduction

Concrete piles are often used to resist earth pressure and to stabilise the soil in slope engineering. However, due to some factors, such as raining and overloading, the initial stable state of a soil slope may change, even leading to soil sliding within the slope. During a mechanical state change, a concrete pile will often undergo horizontal deformation, which will endanger the concrete pile. Moreover, the degradation of the concrete pile will compromise the safety of the soil slope. Therefore, a reliable, effective long-term deformation-monitoring method is needed to ensure the safety of horizontally loaded piles [1,2].

Linear-variable differential transformers (LVDTs) [3], inclinometers [4–6], and vibrating-wire strain gauges (VWSGs) are usually used in the deformation monitoring of concrete piles [7,8]. The horizontal deformation at the pile top can be directly measured with an LVDT with high accuracy [3]. However, LVDTs are not suitable for long-term monitoring because support is needed to install the instruments. Moreover, the horizontal deformation distribution along the pile in the soil cannot be obtained with LVDTs. An inclinometer is often applied to measure the inclination of a pile [4,6]. Horizontal deformation can be assessed using the inclination distribution results, but its accuracy should still be improved to satisfy the monitoring demands. Compared with resistance strain gauges, VWSGs exhibit better strain measurement accuracy and stability. They are commonly used for the strain monitoring of piles [7]. However, due to the limitation in the number of strain measurement points, the accuracy of horizontal deformation measurement should also be further enhanced. The use of many VWSGs will considerably increase costs. In conclusion, there is some difficulty in measuring the horizontal deformation distribution along a pile with the traditional methods if some detailed health of the pile needs to be assessed.

Meanwhile, substantial progress has been obtained in distributed optical-fibre sensing technology, such as Brillouin optical time-domain analysis (BOTDA) [9,10] and Brillouin optical frequency-domain analysis (BOFDA) [11]. Since it was proposed for engineering measurements in 1989, BOTDA has been applied to monitor various geotechnical structures, such as piles, slopes, retaining walls, and excavations, with high strain measurement accuracy and spatial resolution [12–16]. In these applications, the strain distribution can be obtained with an accuracy of about several $\mu\varepsilon$ to more than 20 $\mu\varepsilon$, which should be improved when it is applied to identify some small structure changes, such as the early stage of concrete cracking, or a small loading change. Luckily, the measurement of the strain distribution provides a whole detailed understanding of the monitored structure. However, due to limitations in its spatial resolution (about 10 cm to 50 cm), a nonuniform distribution of the strain within the spatial resolution greatly decreases the strain measurement accuracy of BOTDA. Therefore, a new BOTDA-based long-gauge sensor was proposed, which was first proposed for making distributed long-gauge fibre Bragg grating (FBG) sensors [17]; it was packaged with a fibre-reinforced polymer (FRP) [18], and the gauge length reached 30 cm. The strain distribution within the gauge length was uniform, so strain measurement accuracy was guaranteed. Some research about FBG-FRPs was also implemented to verify the advantage of FRP-packaged optical-fibre sensors, such as embedding FBG-FRPs inside the cable to monitor the distributed cable force [19] and identifying the thermomechanical strain of carbon FRPs (CFRPs) with embedded FBG sensors [20]. The above research has proven that FRP-packaged distributed optical-fibre sensors can implement an accurate strain distribution measurement inside a concrete structure. However, there is little research on deformation assessment with sensing technology.

As a pile is buried in the soil, the long-term monitoring of the deformation distribution along the pile is important in assessing the structural condition of the pile. However, the traditional method presents some difficulty due to technological or economic problems. Therefore, a new method based on distributed optical-fibre sensing technology is proposed for the long-term monitoring of the horizontal deformation of concrete piles with FRP-packaged distributed optical-fibre sensors. In the proposed method, the deformation distribution along the pile can have its novelty assessed using the distributed strain measurement. Considering the excellent long-term performance and low cost of FRP-packaged sensors, the proposed method solves these problems for piles as suggested. To implement this method, the theory of strain deformation conversion is constructed based on the basic beam theory. Then, it is verified via some static experiments of the pile model through a finite element (FE) analysis with a pile specimen in a laboratory.

2. Introduction to FRP-Packaged Distributed Optical-Fibre Sensors

2.1. Strain-Sensing Principle

As shown in Figure 1, a pulse laser (pump laser) and a continuous laser source (probe laser) are introduced into the optical fibre from both ends. When the frequency difference between the two lasers is equal to the Brillouin frequency shift, Brillouin amplification (stimulated Brillouin scattering) occurs in which the two lasers transfer energy [21]. Brillouin scattering is then collected and analysed by a receiver. The central frequency of Brillouin scattering presents a linear relationship with the strain change. Moreover, Brillouin scattering can happen theoretically at each position along the optical fibre. Therefore, distributed strain sensing can be implemented along the optical fibre.

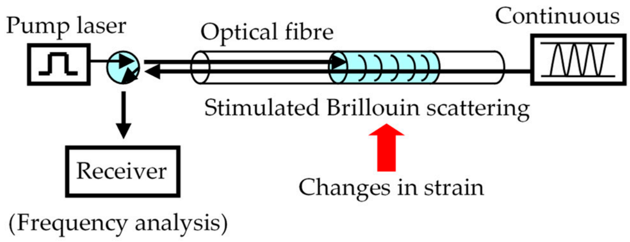

Figure 1. Strain-sensing principle of BOTDA.

In BOTDA, the spatial resolution (often about 10 cm) is a key parameter influencing the application effects of the strain distribution measurement. A nonuniform distribution of the strain within the spatial resolution greatly decreases the strain measurement accuracy of BOTDA as shown in Figure 2a. Therefore, improvement is needed to increase strain measurement accuracy, especially around concrete cracks.

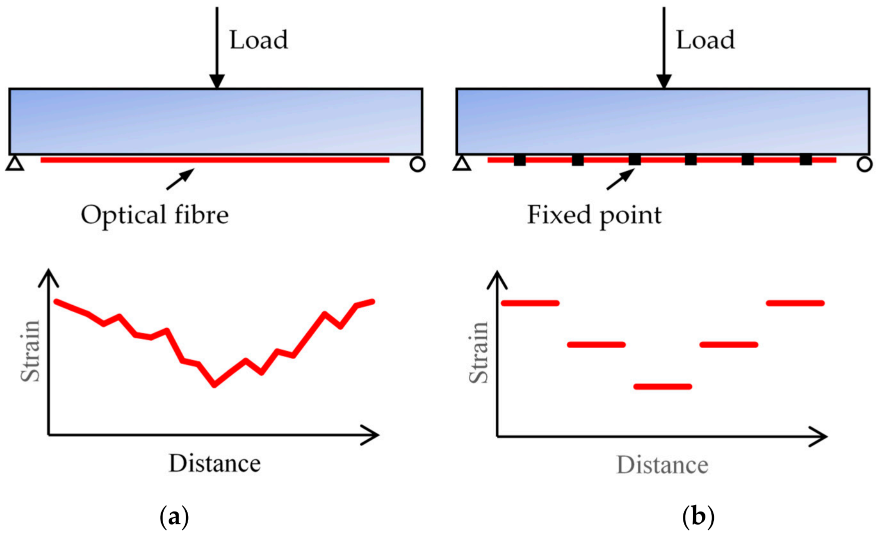

Figure 2. Strain measurement type of (**a**) overall bonding and (**b**) fixed-point bonding.

In actual applications, optical-fibre sensors are often installed via fixed-point bonding [22] as shown in Figure 2b. The strain is distributed uniformly along the optical fibre between the two fixed points, even when the strain of the structure is distributed nonuniformly due to concrete cracks. Thus, the strain measurement accuracy of optical-fibre sensors based on BOTDA can be increased for concrete structures, even in cases with cracks developing. The type of sensor is called a long-gauge optical-fibre sensor. The long-gauge style might slightly decrease sensitivity in cases with small local strain changes, but it is important to ensure basic strain measurement accuracy.

2.2. FRP-Packaged Distributed Optical-Fibre Sensors

Optical fibres are made of glass, so they may be easily broken when used without any special protection in civil engineering. Due to its excellent durability, high strength, and easy manufacture, an FRP is selected in this study as a protective material for optical-fibre sensors. Moreover, an FRP is a typical linear elastic material; it resists residual deformation and prevents a deformation lag upon the sensors. As shown in Figure 3, a distributed optical-fibre sensor is embedded into an FRP bar, forming the proposed long-gauge sensor.

Here, a basalt FRP (BFRP) is applied due to some advantages, especially its sensing purpose. The ultimate strain of a BFRP is much larger than that of a CFRP, which helps the sensor monitor a large strain in some special conditions, like seriously damaged structures. The thermal expansion coefficient of a BFRP is much closer to concrete than that of a CFRP, decreasing the stress caused by a temperature change [23]. It is also found that a BFRP has a higher compressive strength, Young's modulus, and flexural strength than those of an

E-glass FRP. When compared with S-glass and carbon fibres, the basalt fibre shows lower mechanical properties. However, S-glass and carbon fibres are much more expensive than the basalt fibre, which makes the basalt fibre more applicable. Moreover, the resistance of a BFRP to the alkali environment inside concrete structures is not as excellent as that of a CFRP, but it is still good enough to keep the optical fibres inside the BFRP stable [24,25]. The fatigue performance may also be a problem for a BFRP when it is compared with a CFRP. Luckily, the static loading state is the main loading mode when a BFRP-packaged optical-fibre sensor is applied to monitoring a pile.

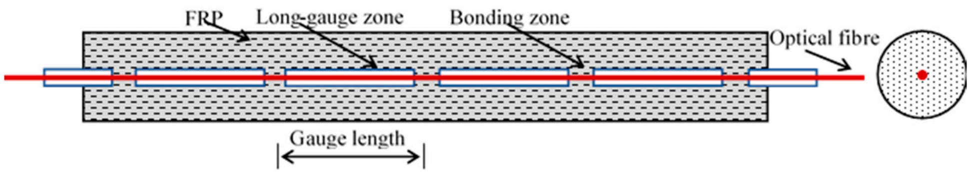

Figure 3. FRP-packaged distributed optical-fibre sensor.

The diameter of a BFRP bar applied to packaged optical-fibre sensors is usually from 6 mm to 10 mm. The size of a BFRP bar cannot be too large to decrease the cost of the sensor package and to avoid the strain-transferring problem. Moreover, the size cannot be too small to keep the bar strong enough to survive the concrete pile construction process. From the previous research, the size of a BFRP bar, as mentioned above, shows no obvious influence on the strain-sensing performance [23]. Considering the environment of the construction field, a diameter of 10 mm is suggested and selected for the BFRP bar in this paper.

An optical-fibre sensor is bonded with an FRP bar via two bonding zones that are each about 5 cm long. Meanwhile, the optical fibre is not bonded with the FRP within the long-gauge zone, thus making the strain distribute uniformly along the optical fibre. The length of the long-gauge zone is often set as 25 cm to ensure that the optical fibre is long enough to sense the average strain of the gauge length considering a spatial resolution of 10 cm for BOTDA. Therefore, the total gauge length is about 30 cm. If the gauge length is too large, the average strain will not easily reflect the local damage. Moreover, some prestrain is applied to the optical fibre, especially for measuring the compressive strain.

The strain-sensing performance of the proposed FRP-packaged distributed optical-fibre sensor is investigated via static tensile tests, and the typical results are shown in Figure 4. Detailed information about the tests and other results can be found in a previous paper [18]. In Figure 4a, a platform is found in the middle of the data curve which contains five strain measurement points. Considering that the sampling interval is 5 cm, the length of the platform is equal to the long-gauge zone length. Meanwhile, the strain at the two ends of one sensing gauge cannot be measured with satisfactory accuracy due to the complicated strain distribution along the bonding zone. Therefore, strain averaging is implemented on the strain results of the platform. A good strain-sensing performance, specifically excellent sensing linearity, good repeatability, and high accuracy, is observed in Figure 4b.

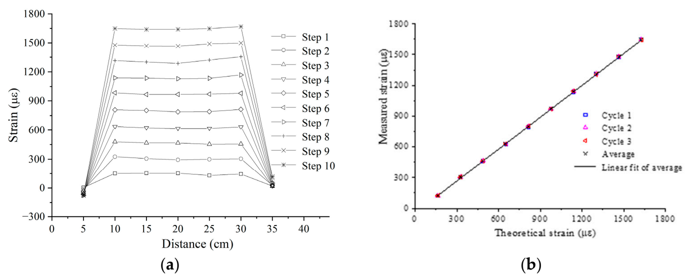

Figure 4. The (**a**) strain distribution and (**b**) strain-sensing accuracy of the proposed sensor.

3. Distributed Deformation Monitoring of Concrete Piles under Horizontal Loads Based on Distributed Strain Sensing

Concrete piles are often buried deeply enough to stop landslides as shown in Figure 5a. However, due to some unexpected factors, such as flooding, slide deformation may happen inside a slope before its collapse. In this case, the pile encounters horizontal loads from the soil. The pile structure can be simplified as a typical Winkler beam model as shown in Figure 5b. In this model, the bottom end of the beam (node N_0) is considered to be a fixed support, which means that there is no horizontal deformation. This assumption is reasonable, as sliding often happens at the upper part of the pile.

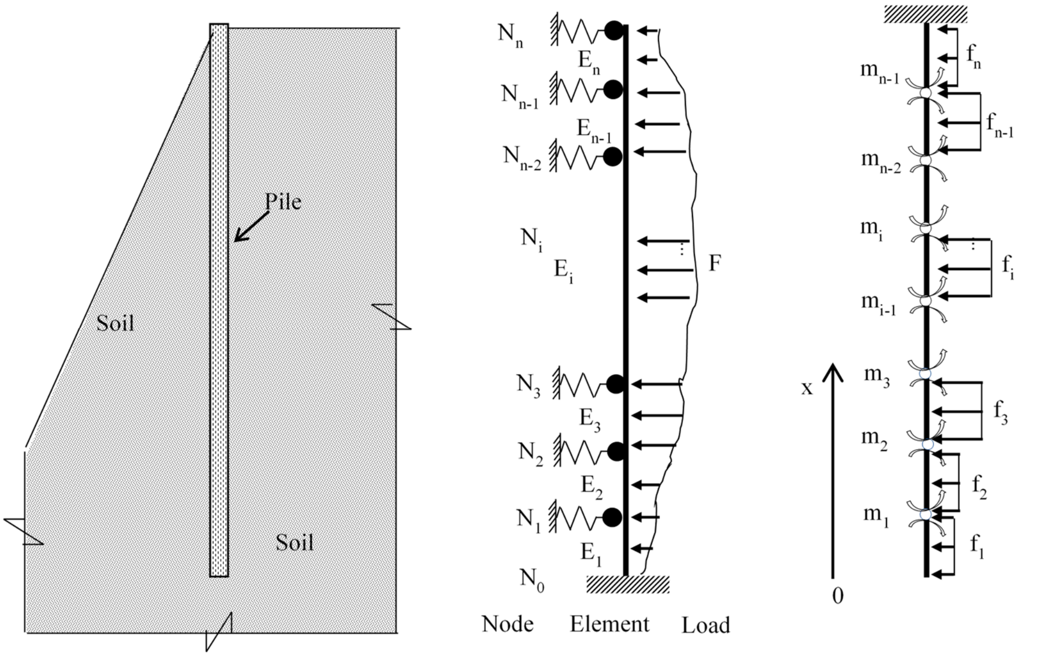

(**a**) (**b**) (**c**)

Figure 5. Pile structure in a slope and its calculation model: (**a**) pile structure, (**b**) simplified model of pile, and (**c**) conjugate model.

In Figure 5b, the pile model is divided into n elements, namely, E_1 to E_n. Each element has the same length, which is set to be the same as the sensing gauge length of the proposed FRP-packaged distributed optical-fibre sensors when applied to the distributed strain monitoring of piles. At each node, N_i (from N_1 to N_n), except N_0, spring support is applied, which means that some horizontal deformation may occur at the node. In the figure, F is the horizontal load from the soil, which is usually difficult to measure.

For horizontal deformation monitoring, the traditional method, namely, the conjugate beam method [26], is applied to the distributed strain measurement in this paper. In the conjugate beam method, the absolute value of the deformation distribution vertical to the length of the original beam is equal to the absolute value of the moment in the conjugated beam. The conjugated model of the pile structure is shown in Figure 5c. The additional moment, m_i, at the i_{th} node is applied to reflect the landslide-induced possibility of horizontal deformation at the spring support in the original pile model. In the conjugated model, the horizontal load is applied to the conjugated model, whose absolute value is equal to the absolute value of the curvature of the original model. Considering the average strain-sensing style of the proposed optical-fibre sensor, the uniform load, f_i, is applied to each element of the conjugated model as shown in Figure 5c. Meanwhile, the uniform load, f_i, can be expressed by Equation (1) in which ε_i is the average strain of the i_{th} element and y_i is the average distance from the sensor to the neutral axis position. Moreover, the element length is set to be the same as the gauge length of the applied distributed optical-fibre sensor.

$$f_i = \frac{\varepsilon_i}{y_i} \tag{1}$$

In Figure 5c, the bending moment, m_i, at each node can be calculated using Equation (2), where l is the element length, which is often set as the same value for all the elements.

$$m_i = \sum_{j=1}^{i} f_j l (i - j + \frac{1}{2}) l = \sum_{j=1}^{i} (i - j + \frac{1}{2}) f_j l^2 \tag{2}$$

Then, Equation (3) can be obtained by plugging Equation (1) into Equation (2).

$$m_i = \sum_{j=1}^{i} (i - j + \frac{1}{2}) \frac{\varepsilon_j l^2}{y_j} \tag{3}$$

Due to the principle of the conjugate beam method, the deformation, d_i, of the original beam vertical to the beam length at each node is equal to the bending moment of the conjugate beam at the same position as shown in Equation (4).

$$d_i = m_i = \sum_{j=1}^{i} (i - j + \frac{1}{2}) \frac{\varepsilon_j l^2}{y_j} \tag{4}$$

The above equations show that the average strain of each element, ε_i, and the average distance from the sensor to the neutral axis position, y_i, are important parameters in the deformation monitoring of concrete piles. The former is measured with the proposed distributed optical-fibre sensor, while the latter is not easily obtained accurately, especially in cases of concrete cracking. Therefore, another calculation model, namely, a fibre model, is applied to determine the neutral axis position as shown in Figure 6.

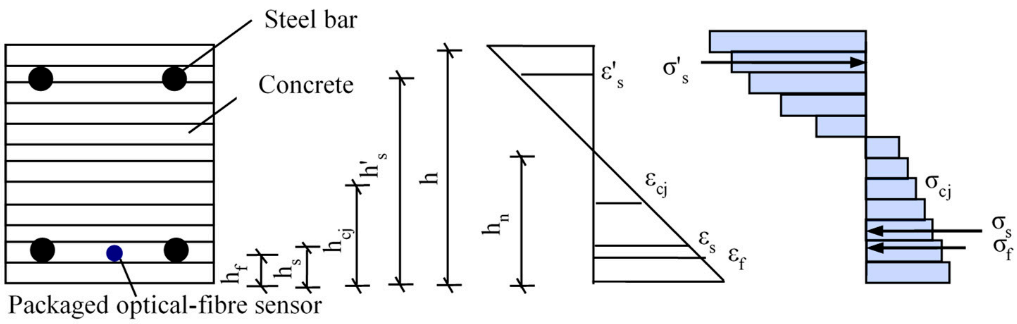

Figure 6. Fibre model for elemental calculation with the input of strain measurements.

In the fibre model, the following assumptions are made: (1) All the parameters used are the average values of the monitored elements along the element length. (2) The plane-section assumption is still right in this model. (3) The stress–strain relationship of the concrete and steel rebar is defined by the Chinese code GB50010-2010 [27]. (4) The stress–strain relationship of the FRP bar is linear. (5) The bond slip between the reinforcement (the steel rebar and FRP bar) and concrete is disregarded.

Horizontal loads are the only loads applied to pile structures during landslides. Here, the self-gravity force is neglected. Therefore, the inner forces vertical to the cross-section of the pile balance; that is, the sum of these inner forces is zero as shown in Equation (5).

$$A_s \sigma_s + A_f \sigma_f + A'_s \sigma'_s + \sum_{j=1}^{n} A_c \sigma_{cj} = 0 \tag{5}$$

With the plane-section assumption, the relationship between the strains can be expressed as Equation (6). For the i_{th} monitored element of the pile, $y_i = h_n - h_f$, and $\varepsilon_i = \varepsilon_f$. Then, Equation (6) can be expressed as Equation (7). As the strain, ε_i, can be obtained by the proposed optical-fibre sensor, there is only one unknown parameter, namely, y_i. The stressors σ_f, σ_s, σ'_s, and σ_{cj} are obtained by taking the strains ε_f, ε_s, ε'_s, and ε_{cj} in the stress–strain relationship of the FRP, steel bar, and concrete. Lastly, y_i is calculated by plugging these stressors into Equation (5).

$$\varepsilon_s = \frac{h_n - h_s}{h_n - h_f}\varepsilon_f, \varepsilon'_s = \frac{h_n - h'_s}{h_n - h_f}\varepsilon_f, \varepsilon_{cj} = \frac{h_n - h_{cj}}{h_n - h_f}\varepsilon_f \tag{6}$$

$$\varepsilon_s = \frac{y_i + h_f - h_s}{y_i}\varepsilon_i, \varepsilon'_s = \frac{y_i + h_f - h'_s}{y_i}\varepsilon_i, \varepsilon_{cj} = \frac{y_i + h_f - h_{cj}}{y_i}\varepsilon_i \tag{7}$$

In Figure 6 and Equations (5) and (6), h is the section height; h_f, h_s, h'_s, h_{cj}, and h_n are the distances from the centre of the embedded optical-fibre sensor, tension steel bar, compression steel bar, j_{th} concrete fibre element, and neutral axis to the beam bottom, respectively. ε_f, ε_s, ε'_s, and ε_{cj} are the strains of the packaged optical-fibre sensor, tension steel bar, compression steel bar, and j_{th} concrete fibre element, whereas σ_f, σ_s, σ'_s, and σ_{cj} are the stressors of these parts, respectively. A_f, A_s, A'_s, and A_{cj} are the cross-sectional areas of the packaged optical-fibre sensor, tension steel bar, compression steel bar, and j_{th} concrete fibre element, respectively. In both the stress and strain, the tension is positive, and the pressure is negative. After the parameter y_i is obtained, the deformation can be calculated using Equation (4).

There is a natural gap between the calculation model and the actual pile structure, as the horizontal deformation caused by the shear stress is neglected in this paper, which creates some error for the deformation calculation. However, the deformation caused by the bending stress is considered to be the main part of the horizontal deformation of the pile in a landslide case. Therefore, the error is considered to be only a small error.

Moreover, under some special conditions, the proposed method may present a large error or fail. If the bottom of the pile loosens during a landslide, there will be some rigid body movements that will cause additional horizontal deformation. This deformation cannot be calculated with the proposed method, which can only calculate the deformation caused by stress. Moreover, if some serious damage causes the pile to undergo plastic hinge effects or a fracture, the proposed method may present a much large error.

The proposed method is applied to calculate the bending deformation using the distributed strain. If the bending mode is not the main loading mode for the pile, the proposed method will present a large error or even fail to implement the deformation calculation. If the bending mode is still the main loading mode, no matter the load value or type or the service environment, the proposed method will still be useful. Luckily, in the case of the landside in this paper, the bending mode is the main loading mode for the pile.

4. FE Model Simulation

4.1. Description of FE Model

The concrete pile model was simulated with the FE software Abaqus 2020 under landslide conditions to verify the proposed method. In the model, the concrete, steel, and soil were considered to be elastoplastic materials, while the FRP was considered to be an elastic material. Detailed information about the materials is shown in Table 1. The parameters of the concrete, steel, and soil were from the Chinese code GB50010-2010 [27], while the parameters of the FRP were provided by the manufacturer. The stress–strain relationship of the concrete and steel was defined by the Chinese code GB50010-2010 [27], while the Drucker–Prager (DP) yield criterion was applied for the soil.

Table 1. Mechanical properties of materials.

Material	Elastic Modulus (GPa)	Density (kg/m^3)	Poisson's Ratio	Compressive Strength (MPa)	Tensile Strength (MPa)	Cohesive Force (kPa)	Internal Friction Angle (°)
Concrete	29.8	2500	0.17	20.1	2.01		
Steel	200	7800	0.30	400	400		
FRP	60	2000	0.2	500	1000		
Soil	0.26	1900	0.42			19	31

A three-dimensional solid element (unit C3D8R) was applied to the concrete and soil in the model, while a truss element (unit T3D2) was used for the steel bar and FRP-packaged sensor. The interaction between the concrete and soil was considered to be typical surface–surface contact. The slip between the concrete and steel bar was neglected in the model. The slip between the concrete and the FRP-packaged sensor was also neglected, as there was nearly no obvious debonding happening before the yielding of the steel bar [18]. The interface between the optical-fibre sensor and FRP was fixed in the FE model, namely, no debonding, as the length of the bonding zone, 5 cm, was long enough to cause no interface debonding to happen before the sensing failure.

The piles were positioned in a row along the slope at certain intervals. In this paper, the spacing was 3.2 m, which was obtained from an actual slope. Therefore, in the simulation model, the depth of the model was set as 3.2 m, and one pile was set in the middle. Figure 7a presents the details of the geometric model. For the pile, the length was 18.5 m, and its section was a square with a side length of 0.8 m. The FRP-packaged sensor was installed along the steel bar to obtain the strain distribution, as shown in Figure 7b, for which the gauge length was 30 cm. Moreover, the BFRP was applied here.

For the simulation, the FE model was constructed as shown in Figure 7c. In the model, the mesh size was 100 mm for the reinforcement, while it was 40 mm for the concrete. In the model, the strength reduction method was applied to simulate the landslide [28]; the cohesion and internal friction angle of the soil were reduced through a specific reduction formula, and the model was recalculated until the instability case happened according to the Mohr–Coulomb criterion. The strain distribution along the FRP-packaged sensor was extracted from the model for each case. Then, the results were plugged into the proposed equations, which are presented in the above chapter, to calculate the horizontal deformation distribution of the pile. For comparison, the horizontal deformation along the pile was also extracted from the model.

4.2. FE Simulation Results

Figure 8 presents the typical results of the FE simulation from which the landslide surface can be easily identified. The greatest damage to a pile occurs near the slide surface. The applicability of the proposed method was verified by extracting the results of the loading cases to implement the analysis, namely, Case 1 (concrete before cracking), Case 2 (concrete after cracking (reinforcing steel bar before yielding)), and Case 3 (reinforcing steel bar after yielding) as shown in Figure 9.

The axial strain of the FRP-packaged sensor at the tensile side was extracted as the strain-monitoring value as shown in Figure 9. From the strain distribution, the damage zone can be identified. In Case 1, there are not too many differences along the strain distributes of the pile among which the largest strain is about 100 $\mu\varepsilon$, meaning no concrete cracking. In Case 2, the strain increases greatly, especially along the length from 6 m to 10 m, where the largest strain is more than 1000 $\mu\varepsilon$, indicating that some large concrete has developed. In Case 3, the large strain zone expands from 5.5 m to 11.5 m, and the largest strain is up to 2000 $\mu\varepsilon$, indicating the occurrence of reinforcement yielding. From the results of the strain distribution, it can also be found that the distributed strain measurement can identify where the damage happens, as the damage lies locally.

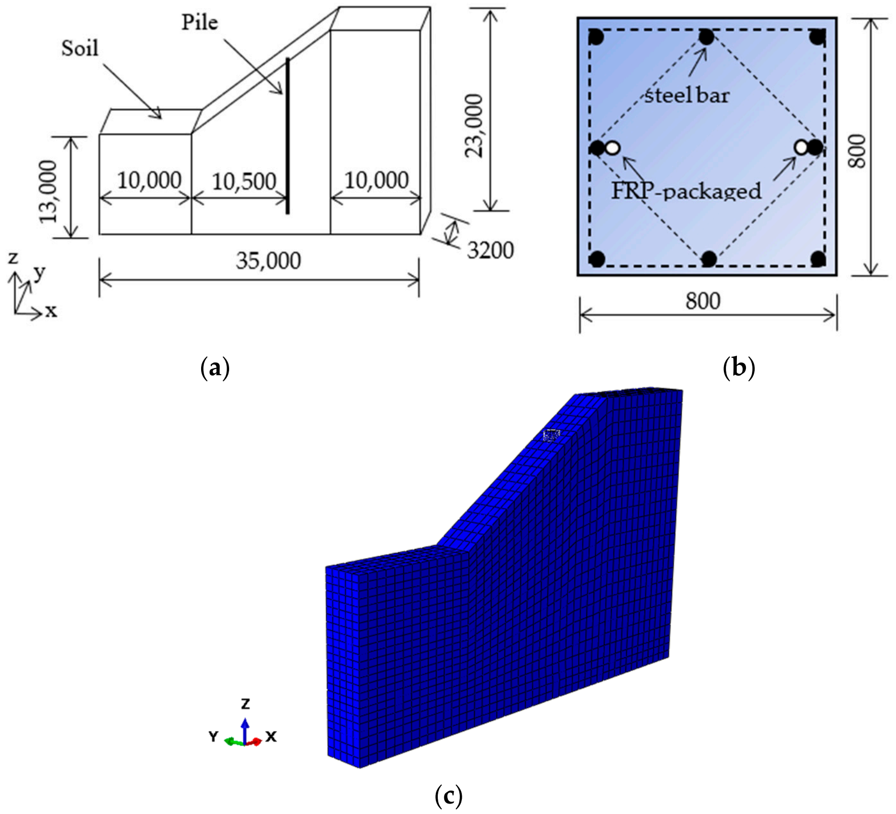

Figure 7. Detailed information of the model: (**a**) geometric model, (**b**) pile section, and (**c**) FE model (unit: mm).

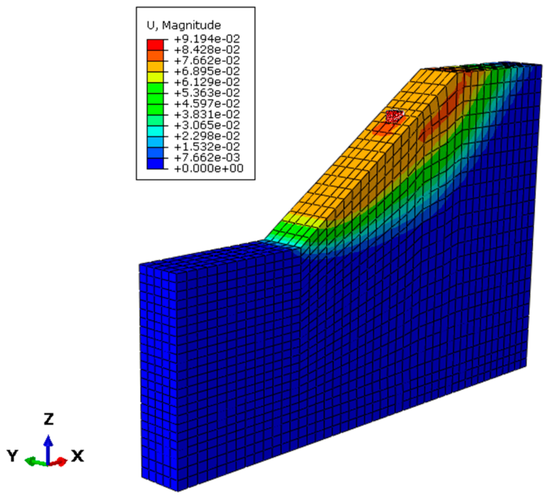

Figure 8. Typical results of x-direction deformation of FE simulation.

4.3. Verification of Deformation Calculation

The strain results were inputted into the proposed method to calculate the horizontal deformation distribution of the pile. The results of the horizontal deformation distribution of the pile can be directly extracted from the FE model, which is considered to be the true value. The deformation results are presented in Figure 10a. The horizontal deformation is largest at the top of the pile, and it decreases greatly along the depth until reaching the slide surface. The horizontal deformation of the parts of the pile below the slide surface is small and changes only slightly with the loading case. The results also indicate that the calculated deformation is close to the true value, even after the steel bar yields. However, an evident error develops with the loading case. As shown by the results in Figure 10b, the error increases with the deformation, and it is largest at the top of the pile. Nonetheless, the relative value of the larger error is still about only 10%, which can be accepted in civil engineering. A partial reason for this error is the difference between the calculation model and the actual structure. In addition, the great damage may have changed the deformation type. For Case 3, due to the great damage from the steel bar yielding, some rigid body movements may have caused the calculation error to increase greatly for the pile parts above the damage zone. Therefore, the proposed method should be further improved to consider such great damage to increase the calculation accuracy.

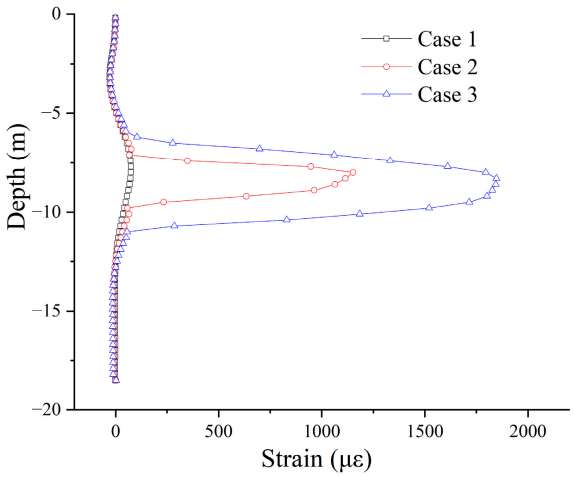

Figure 9. Results of strain.

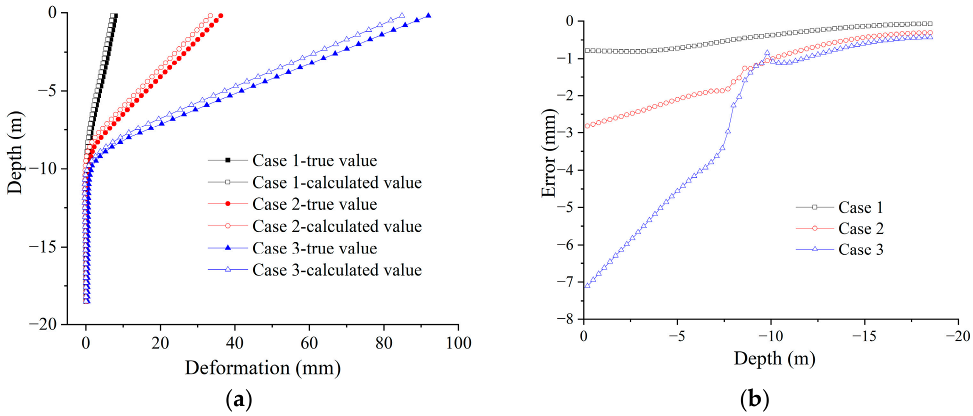

Figure 10. The (**a**) deformation results and (**b**) calculation error of FE model.

5. Static Experiments of Concrete Pile Specimen

5.1. Description of Experiments

In this paper, a concrete pile was subjected to static loads as shown in Figure 11a. Due to the limitations imposed by the laboratory conditions, the landslide could not be easily simulated. Therefore, some horizontal loads were applied to a scale model of the concrete pile to verify the sensing performance and assessment accuracy of the proposed method.

In the tests, the concrete pile specimen was affixed to a steel bucket filled with soil to simulate an actual soil foundation. According to the tests, the average compressive strength of the concrete was 43.21 MPa, while the elastic modulus was 32.5 GPa. The pile model had a length of 1.8 m and had a square section. The length of each side of the section was 0.2 m. There was one steel bar with a diameter of 12 mm at each corner of the section.

One FRP-packaged sensor was installed in the middle of the sideline of the section, while another sensor was installed at the same position at the opposite sideline. During the tests, the largest tension and compressive strain occurred at the two sidelines. The diameter of the sensor was about 10 mm, and the gauge length was 300 mm. In total, there were five sensing gauges as shown in Figure 11b. Accordingly, the pile was divided into five elements for monitoring, namely, Element 1 to Element 5; one element (Element 0) was set for loading as shown in Figure 11a. For comparison, one traditional strain gauge was bonded at the surface of the FRP-packaged sensor in the middle of each sensing gauge. Meanwhile, some deformation metres were installed at the surface of the pile at some nodes (Node 1, Node 2, and Node 3) to measure the horizontal deformation as shown in Figure 11a.

During the loading tests, the data of the optical-fibre sensor were collected by the distributed optical-fibre sensing system (Figure 11c) NBX-6050 (Neubrex Co, Ltd, Tokyo, Japan). The strain measurement accuracy of the system could reach 7.5 $\mu\varepsilon$, while the largest sensing length could be up to 20 km. In the tests, loading was applied to the step of the referenced horizontal deformation. The deformation measured by metre #1 is the referenced deformation. The test was terminated after the steel bar yielded.

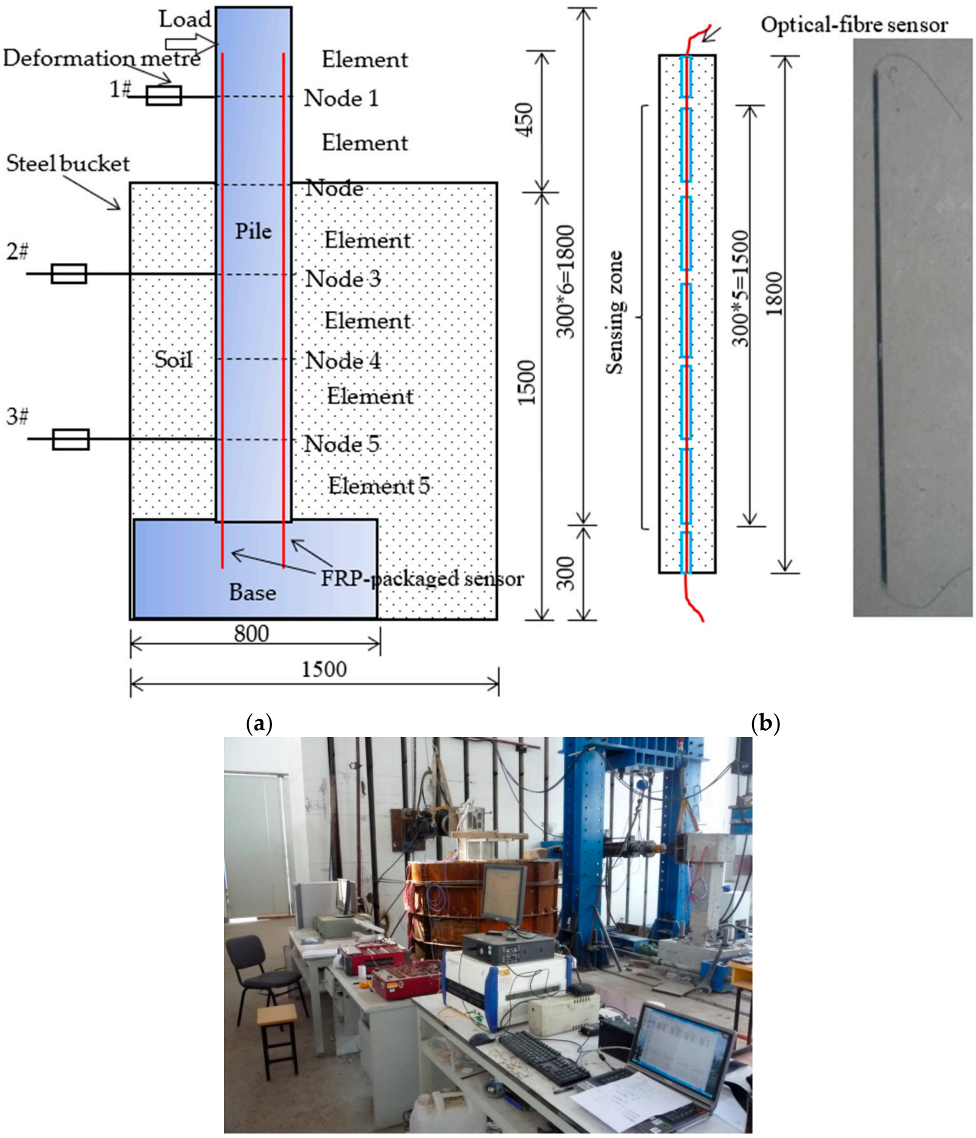

Figure 11. Description of model test: (**a**) specimen and test setup, (**b**) FRP-packaged sensor, and (**c**) test field (unit: mm).

5.2. Experimental Results and Analysis

5.2.1. Strain Measurement Results

The strain measurements obtained by the optical-fibre sensor are presented in Figure 12. According to the results, the largest strain happened at Element 4 of the pile model due to the confines of the surrounding soil. Therefore, concrete cracking and reinforcement yielding occurred easily within Element 4. Another discovery is that the strain at the compressive side is much smaller than that at the tensile side, especially in the large-load case. One reason is that the concrete cracks at the tensile side made the neutral axis move toward the compressive side, which made the strain increase at the compressive side less than at the tensile side. Furthermore, the prestrain loss within the optical-fibre sensor may have made the sensor fail to further measure the compressive strain, as was the case for Element 2 and Element 3. Therefore, the strain measurements obtained by the optical-fibre sensor at the tensile side are much more reliable that those at the compressive side. The strain measurement results at the tensile side were also used in the deformation calculation in this paper.

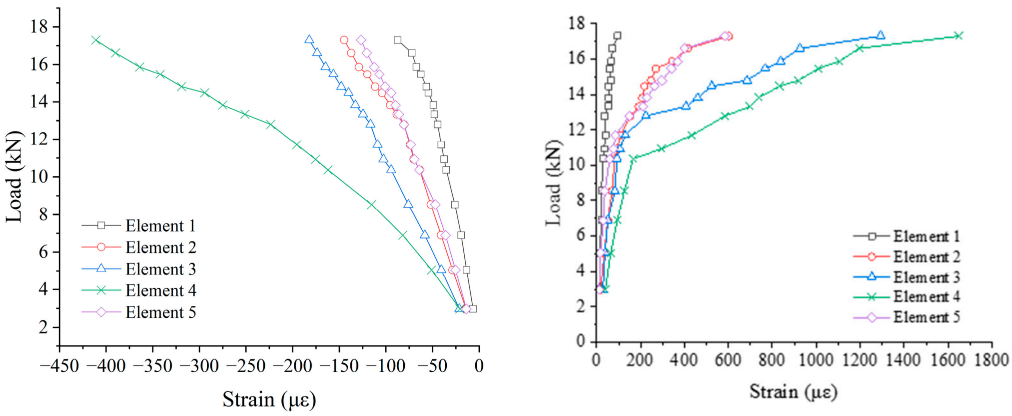

Figure 12. The strain measurement results (**a**) at the compression side and (**b**) at the tension side obtained by optical-fibre sensors.

Traditional strain gauges were applied in the tests to assess the strain measurement performance of the proposed FRP-packaged distributed optical-fibre sensor. Some of the typical results at the tensile side were extracted and are compared in Figure 13. The strain measurements from the optical-fibre sensor are generally close to those from the strain gauge, but the largest measurement difference is 200 με. One important reason for this difference is that the strain gauge was installed on the surface of the FRP-packaged sensor, while the optical-fibre sensor was inside the sensor. Another reason is that local damage, such as concrete cracks, may have exerted a more noticeable influence on the strain gauge, as the optical-fibre sensor measured the average strain change along the sensing gauge length.

5.2.2. Results of Horizontal Deformation

The measured strain results were inputted into the proposed method to calculate the horizontal deformation distribution of the concrete pile. The calculated deformation results, as shown in Figure 14, indicate that the horizontal deformation is largest at the top of the pile model and then decreases greatly toward the bottom. The distribution agrees with the theoretical distribution, which indicates the validity of the proposed method.

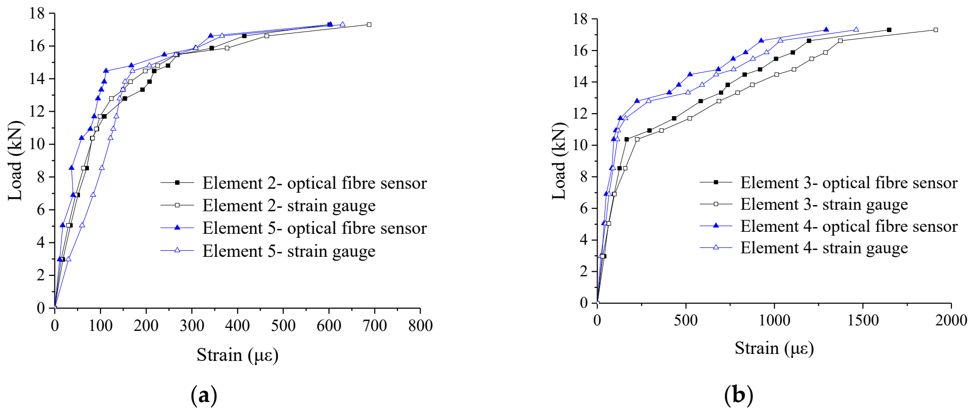

Figure 13. Typical comparison results of different strain-sensing methods: (**a**) Element 2 and Element 5 and (**b**) Element 3 and Element 4.

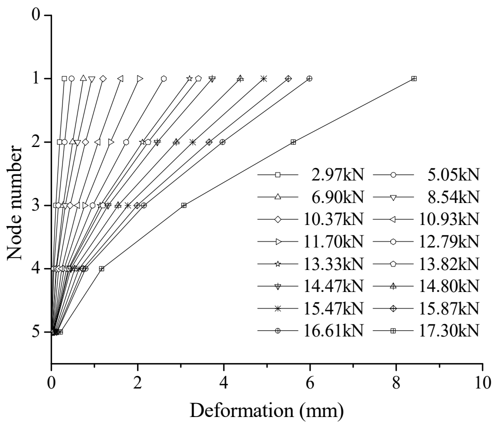

Figure 14. The results of horizontal deformation distribution.

5.3. Verification of Deformation Calculation

For further evaluation of the performance of the proposed method, the deformation results obtained by the optical-fibre sensor were compared with those obtained by the traditional metre, which were considered the true value of the horizontal deformation. From the results in Figure 15, it is found that the measured deformation values from the two types of sensing methods are close to each other, even in the large-deformation case of steel yielding. The measurement error was calculated and is presented in detail in Figure 16. The absolute error increases with the deformation as shown in Figure 16a, and the largest error is about 1.2 mm in the largest-deformation case at Node 1. By contrast, the absolute value of the relative error decreases with an increase in the deformation as shown in Figure 16b. The relative error of the horizontal deformation measurement at the top of the pile model can be limited within 12.5%, especially in the large-deformation case. The primary reason for such a measurement error is the gap between the theoretical model and the actual structure. However, the large relative error in the small-deformation case may have been mostly caused by the low accuracy of the deformation metre in measuring small deformations and the instability of BOTDA in measuring small strains. Therefore, the calculation model needs to be further modified to improve the measurement accuracy, especially for large deformations, which are important in the assessment of pile safety.

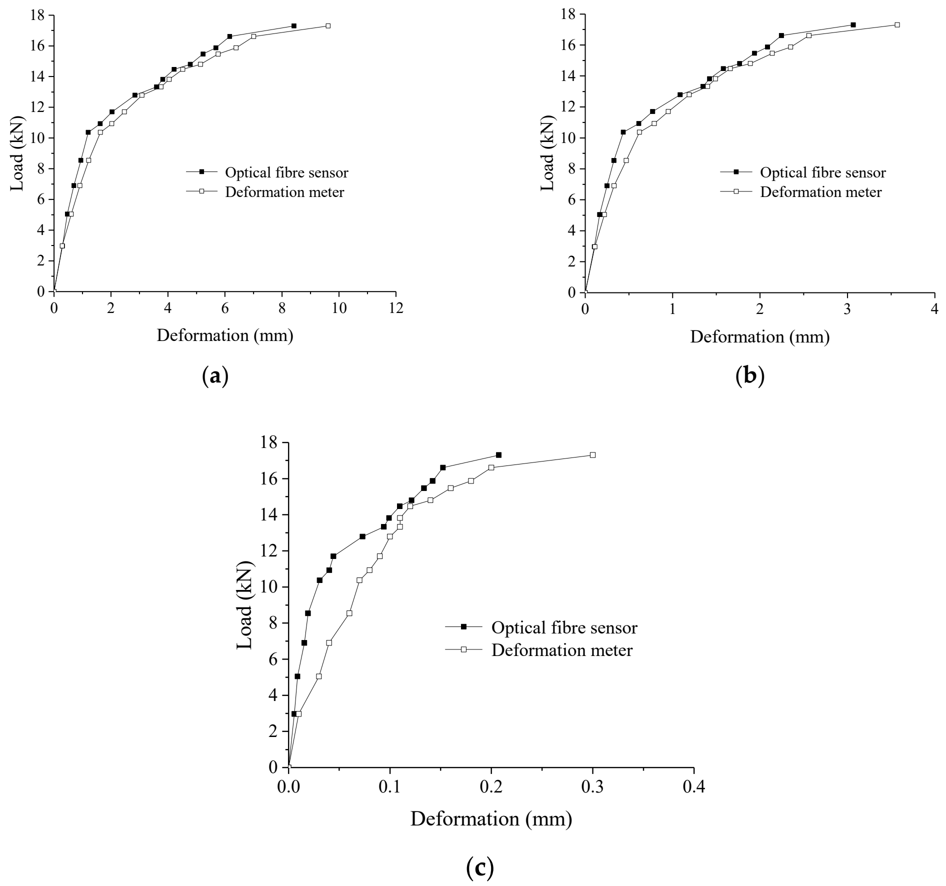

Figure 15. The measurement comparison results of (**a**) Node 1, (**b**) Node 3, and (**c**) Node 5.

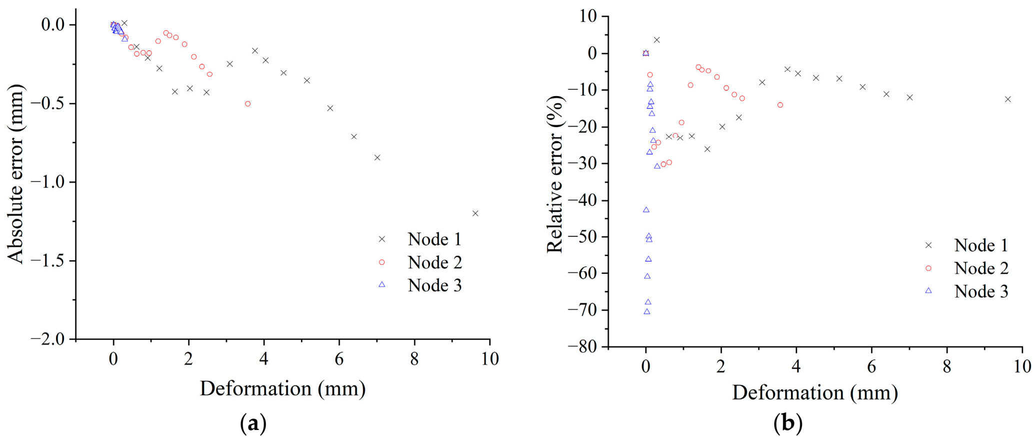

Figure 16. The (**a**) absolute error and (**b**) relative error of horizontal deformation measurement.

6. Conclusions and Remarks

In this paper, distributed strain-sensing technology is applied along with an FRP-packaged long-gauge optical-fibre sensor to measure the strain distribution of concrete piles under horizontal loading. Then, the horizontal deformation distribution can be calculated with the proposed calculation equations. Lastly, the performance of the proposed method is verified via some static experiments on an FE pile model with a pile specimen in a laboratory. The following conclusions are drawn:

(1) The proposed FRP-packaged distributed optical-fibre sensor can be applied to monitor the distributed strain distribution of concrete pile structures, even in great-damage cases, such as reinforcement yielding.

(2) Based on the typical Winkler beam model, the horizontal deformation of a concrete pile can be calculated with the input of the distributed strain measurements, even when considering the development of structural damage, such as concrete cracking and reinforcement yielding.
(3) The proposed method is verified to have good accuracy by the results of the FE simulation and static experiments. Before the case of reinforcement yielding, the deformation measurement error with the proposed method is about 1 mm. It can be up to several millimetres after reinforcement yielding due to the large gap between the calculation model and the actual structure, while the relative measurement error is still about 10%.

Further work is needed to make the proposed method more applicable to pile monitoring. First, the measurement accuracy and range of the sensor should be improved, especially for compressive strain monitoring. Second, the gap between the calculation model and actual pile structures decreases the measurement accuracy of the proposed method, especially after the development of great structural damage. Therefore, the calculation model should be modified to enhance the accuracy of the horizontal deformation assessment of concrete piles in landslide cases.

Considering the excellent long-term monitoring of optical-fibre sensing technology, the proposed method can be effectively applied to the horizontal deformation monitoring of concrete piles.

Author Contributions: Conceptualization, Y.T. and B.L.; data curation, M.C.; formal analysis, M.C.; funding acquisition, B.L.; investigation, X.C. and Z.W.; methodology, Y.T. and B.L.; validation, Y.T., M.C. and Z.W.; writing—original draft, X.C.; writing—review and editing, Y.T. All authors have read and agreed to the published version of the manuscript.

Funding: This research work was funded by the National Key R&D Program of China (Grant No. 2021YFB2601200) from Ministry of Science and Technology of the People's Republic of China and the Jiangsu Transportation Technology and Achievement Transformation Project (Grant No. 2022Y20) from Jiangsu Provincial Department of Transportation.

Data Availability Statement: All data included in this study are available upon request through contact with the corresponding author.

Conflicts of Interest: The authors declare no conflict of interest.

Abbreviations

LVDTs	Linear-variable differential transformers
VWSGs	Vibrating-wire strain gauges
BOTDA	Brillouin optical time-domain analysis
BOFDA	Brillouin optical frequency-domain analysis
FBG	Fibre Bragg grating
FRP	Fibre-reinforced polymer
FE	Finite element

References

1. Pei, H.F.; Teng, J.; Yin, J.H.; Chen, R. A review of previous studies on the applications of optical fiber sensors in geotechnical health monitoring. *Measurement* **2014**, *58*, 207–214. [CrossRef]
2. Yu, P.Y.; Shen, Y.L.; Ren, Y.Z. Long-term performance of a deep excavation in silty clay in Xi'an-A case Study. *Buildings* **2022**, *12*, 1952. [CrossRef]
3. Seo, H. Monitoring of CFA pile test using three dimensional laser scanning and distributed fiber optic sensors. *Opt. Lasers Eng.* **2020**, *130*, 106089. [CrossRef]
4. Zhang, Y.; Hu, X.; Tannant, D.D.; Zhang, G.; Tan, F. Field monitoring and deformation characteristics of a landslide with piles in the Three Gorges Reservoir area. *Landslides* **2018**, *15*, 581–592. [CrossRef]
5. Asua, E.; Feutchwanger, J.; García-Arribas, A.; Etxebarria, V. Sensorless control of SMA-based actuators using neural networks. *J. Intell. Mater. Syst. Struct.* **2010**, *21*, 1809–1818. [CrossRef]

6. Xiang, B.; Zhang, L.M.; Zhou, L.R.; He, Y.Y.; Zhu, L. Field lateral load tests on slope-stabilization grouted pipe pile groups. *J. Geotech. Geoenviron. Eng.* **2015**, *141*, 04014124. [CrossRef]
7. Kershaw, K.A.; Luna, R. Full-scale field testing of micropiles in stiff clay subjected to combined axial and lateral loads. *J. Geotech. Geoenviron. Eng.* **2014**, *140*, 255–261. [CrossRef]
8. Lirer, S. Landslide stabilizing piles: Experimental evidences and numerical interpretation. *Eng. Geol.* **2012**, *149*, 70–77. [CrossRef]
9. Krisada, C.; Nazam, A.; Phatthanayu, P.; Nakhorn, P.; Panuwat, J.; Hisham, M.; Mingliang, Z.; Qudeer, H. Flexural behavior of natural hybrid FRP-strengthened RC beams and strain measurements using BOTDA. *Polymers* **2021**, *13*, 3604.
10. Xu, D.S.; Yin, J.H.; Liu, H.B. A new measurement approach for deflection monitoring of large-scale bored piles using distributed fiber sensing technology. *Measurement* **2018**, *117*, 444–454. [CrossRef]
11. Li, D.N.; Ma, D.S.; Su, D.; Rao, S.H.; Wang, W.B.; Hong, C.Y. Monitoring Axial Force Development in a Super-Long Pile during Construction Using BOFDA and Data Interpretation Approaches: A Case Study. *Buildings* **2022**, *12*, 1462. [CrossRef]
12. Pelecanos, L.; Soga, K.; Chunge, M.P.M.; Ouyang, Y.; Kwan, V.; Kechavarzi, C.; Nicholson, D. Distributed fibre-optic monitoring of an Osterberg-cell pile test in London. *Géotech. Lett.* **2017**, *7*, 152–160. [CrossRef]
13. Mohamad, H.; Soga, K.; Pellew, A.; Bennett, P.J. Performance monitoring of a secant-piled wall using distributed fiber optic strain sensing. *J. Geotech. Geoenviron. Eng.* **2011**, *137*, 1236–1243. [CrossRef]
14. Motamedi, M.H.; Feng, X.; Zhang, X.; Sun, C.; Ansari, F. Quantitative investigation in distributed sensing of structural defects with Brillouin optical time domain reflectometry. *J. Intell. Mater. Syst. Struct.* **2012**, *24*, 1187–1196. [CrossRef]
15. Hong, C.Y.; Zhang, Y.F.; Liu, L.Q. Application of distributed optical fiber sensor for monitoring the mechanical performance of a driven pile. *Measurement* **2016**, *88*, 186–193. [CrossRef]
16. Zhou, Z.; He, J.; Chen, G.; Ou, J. A smart steel strand for the evaluation ofprestress loss distribution in post-tensioned concrete structures. *J. Intell. Mater. Syst. Struct.* **2009**, *20*, 1901–1912. [CrossRef]
17. Tang, Y.S.; Wu, Z.S.; Yang, C.Q.; Wu, G. A model-free damage identification method for flexural structures using dynamic measurements from distributed long-gage macro-strain sensors. *J. Intell. Mater. Syst. Struct.* **2014**, *25*, 1614–1630. [CrossRef]
18. Tang, Y.S.; Wu, Z.S. Distributed long-gauge optical fiber sensors based self-sensing FRP bar for concrete structure. *Sensors* **2016**, *16*, 286. [CrossRef]
19. Zhou, G.; Zhang, Z.; Ren, L.; Li, D.; Zhao, X. Design of smart cable for distributed cable force measurement in cable dome structures and its application. *Buildings* **2023**, *13*, 2186. [CrossRef]
20. Shafighfard, T.; Mieloszyk, M. Model of the temperature influence on additively manufactured carbon fibre reinforced polymer samples with embedded fibre Bragg grating sensors. *Materials* **2022**, *15*, 222. [CrossRef]
21. Zeni, L.; Picarelli, L.; Avolio, B.; Coscetta, A.; Papa, R.; Zeni, G.; Di Maio, C.; Vassallo, R.; Minardo, A. Brillouin optical time-domain analysis for geotechnical monitoring. *J. Rock Mech. Geotech. Eng.* **2015**, *7*, 458–462. [CrossRef]
22. Zhang, H.; Wu, Z.S. Performance evaluation of BOTDR-based distributed fiber optic sensors for crack monitoring. *Struct. Health Monit.* **2008**, *7*, 143–156. [CrossRef]
23. Tang, Y.S.; Wu, Z.S.; Yang, C.Q.; Wu, G. A new type of smart BFRP bars as both reinforcements and sensors for civil engineering application. *Smart Mater. Struct.* **2010**, *19*, 115001. [CrossRef]
24. Wu, G.; Dong, Z.Q.; Wang, X.; Zhu, Y.; Wu, Z.S. Prediction of long-term performance and durability of BFRP bars under the combined effect of sustained load and corrosive solutions. *J. Compos. Constr.* **2015**, *19*, 04014058. [CrossRef]
25. Ali, A.H.; Mohamed, H.M.; Benmokrane, B.; Adel ElSafty, A.; Chaallal, O. Durability performance and long-term prediction models of sand-coated basalt FRP bars. *Compos. Part B Eng.* **2018**, *157*, 248–258. [CrossRef]
26. Abdul-Shafi, A.K. Solutions Using Conjugate Elements. *J. Struct. Div.* **1980**, *106*, 1–5. [CrossRef]
27. *GB50010-2010*; Code for Design of Concrete Structure. Ministry of Housing and Urban–Rural Development of the People's Republic of China. Code of China: Beijing, China, 2010.
28. Wu, S.C.; Xiong, L.F.; Zhang, S.H. Strength reduction method for slope stability analysis based on a dual factoring strategy. *Int. J. Geomech.* **2018**, *18*, 04018123. [CrossRef]